Resonant interactions in bouncing droplet chains

Lauren Barnes, Giuseppe Pucci, Anand U. Oza

INSTITUT DE FRANCE
Académie des sciences

Comptes Rendus
Mécanique

Lauren Barnes, Giuseppe Pucci and Anand U. Oza

Resonant interactions in bouncing droplet chains

Volume 348, issue 6-7 (2020), p. 573-589.

<https://doi.org/10.5802/crmeca.30>

Part of the Thematic Issue: Tribute to an exemplary man: Yves Couder

Guest editors: Martine Ben Amar (Paris Sciences & Lettres, LPENS, Paris, France), Laurent Limat (Paris-Diderot University, CNRS, MSC, Paris, France), Olivier Pouliquen (Aix-Marseille Université, CNRS, IUSTI, Marseille, France) and Emmanuel Villermaux (Aix-Marseille Université, CNRS, Centrale Marseille, IRPHE, Marseille, France)

Les Comptes Rendus. Mécanique *sont membres du Centre Mersenne pour l'édition scientifique ouverte*
www.centre-mersenne.org

Comptes Rendus
Mécanique
2020, 348, nº 6-7, p. 573-589
https://doi.org/10.5802/crmeca.30

Tribute to an exemplary man: Yves Couder

Bouncing drops, memory

Resonant interactions in bouncing droplet chains

Lauren Barnes [a], Giuseppe Pucci [b] and Anand U. Oza [*, c]

[a] Department of Mathematical Sciences, New Jersey Institute of Technology, Newark, New Jersey 07102, USA

[b] Université de Rennes 1, CNRS, IPR (Institut de Physique de Rennes) UMR 6251, F-35000 Rennes, France

[c] Department of Mathematical Sciences & Center for Applied Mathematics and Statistics, New Jersey Institute of Technology, Newark, New Jersey 07102, USA

E-mails: lgb5@njit.edu (L. Barnes), giuseppe.pucci@univ-rennes1.fr (G. Pucci), oza@njit.edu (A. U. Oza)

Abstract. In a pioneering series of experiments, Yves Couder, Emmanuel Fort and coworkers demonstrated that droplets bouncing on the surface of a vertically vibrating fluid bath exhibit phenomena reminiscent of those observed in the microscopic quantum realm. Inspired by this discovery, we here conduct a theoretical and numerical investigation into the structure and dynamics of one-dimensional chains of bouncing droplets. We demonstrate that such chains undergo an oscillatory instability as the system's wave-induced memory is increased progressively. The predicted oscillation frequency compares well with previously reported experimental data. We then investigate the resonant oscillations excited in the chain when the drop at one end is subjected to periodic forcing in the horizontal direction. At relatively high memory, the drops may oscillate with an amplitude larger than that prescribed, suggesting that the drops effectively extract energy from the collective wave field. We also find that dynamic stabilization of new bouncing states can be achieved by forcing the chain at high frequency. Generally, our work provides insight into the collective behavior of particles interacting through long-range and temporally nonlocal forces.

Keywords. Pilot-wave hydrodynamics, Walking droplets, Nonlinear dynamics, Drop interactions, Collective dynamics, Non-equilibrium systems.

1. Introduction

The seminal experiments of Yves Couder, Emmanuel Fort and collaborators demonstrated that millimetric droplets bouncing on a vibrating fluid bath exhibit behaviors previously thought

* Corresponding author.

to be peculiar to the microscopic quantum realm. While *bouncers* impact the same location on the liquid interface [1, 2], *walkers* are propelled along the interface by the pilot-wave field they generate [3, 4], provided the vibrational forcing acceleration of the bath is sufficiently large. These walkers, which comprise both the droplet and its self-generated wave field, offer an intriguing visualization of wave-particle coupling on a macroscopic scale [4]. They have been shown to exhibit a number of quantum mechanical analogues, including tunneling [5], quantized Larmor levels [6, 7], double quantization in a harmonic potential [8–10], Zeeman-like splitting [11], multimodal statistics in circular corrals [12, 13], statistical projection effects in elliptical corrals [14], Friedel oscillations [15], and the Hong–Ou–Mandel effect [16]. Analogues of single- and double-slit diffraction [17] remain the subject of ongoing investigation [18–23]. The relation between this hydrodynamic system and quantum pilot-wave theories has been reviewed elsewhere [24–26].

A key feature of the walker system is its *path memory*, as the walker's trajectory is influenced by the waves it generates during its prior impacts [6, 27]. These waves are sustained by the vibrational forcing of the bath. While single droplets are influenced by their own history, collections of bouncers and walkers may interact through the collective wave field they generate. Lattices of bouncers have been shown to arrange themselves into eight of the eleven possible Archimedean tilings of the plane [28], and both stationary and spontaneously spinning droplet lattices have been reported [29–31]. Rectangular and hexagonal lattices of bouncers exhibit oscillatory instabilities that arise as the bath's vibrational acceleration is increased progressively [32], with propagating oscillations that are reminiscent of phonons in crystalline solids [33]. More recently, a hydrodynamic spin lattice was obtained by confining walkers using an array of circular wells submerged in a relatively shallow liquid layer [34, 35]. Each walker executes roughly circular motion in its own well, but the motions become more correlated as the bath's forcing acceleration is increased progressively, the result being a large-scale collective dynamics with either antiferromagnetic or ferromagnetic order.

In addition to the two-dimensional lattices described above, one-dimensional rings and chains of bouncers and walkers have been shown to exhibit rich phenomenology. Strings of up to eleven walkers confined to a circular annulus move faster than an individual walker, with the speed increasing with the number of walkers [36, 37]. Thomson *et al.* [38, 39] demonstrated that a ring of twenty bouncers confined within an annulus may exhibit small-amplitude binary oscillations, whereas a ring of forty bouncers exhibits a striking solitary wave-like instability. Free rings of bouncing droplets destabilize into a variety of dynamical states as the bath's forcing acceleration is increased progressively, including steady rotational motion, periodic radial or azimuthal oscillations, azimuthal traveling waves and rearrangement into regular polygonal structures [40]. This body of literature shows that lattices of bouncing droplets exhibit behavior reminiscent of crystal vibrations, which can be profitably clarified and extended by analyzing different ordered arrangements of bouncers.

We present here a theoretical investigation of free one-dimensional chains of bouncing droplets, as depicted in Figure 1(a). Particular attention will be paid to driven droplet chains, in which the drop at one end of the chain is subjected to a time-periodic forcing in the horizontal direction (Figure 1(b)). We note that periodically-driven classical systems, both deterministic [41, 42] and stochastic [43], have a long history of study, and there has been recent interest in driven many-body quantum systems [44, 45]. However, relatively little is known about driven classical systems with temporally nonlocal interactions [46], as arise in droplet chains due to their path memory. While forced bouncing droplet collectives have not yet been studied experimentally, Perrard [47] applied periodic forcing to a single walker by encapsulating a drop of ferrofluid within an oil droplet, and then applying a vertical magnetic field with a radial gradient. By modulating the magnetic field strength, the dynamics of a walker in an oscillatory central force

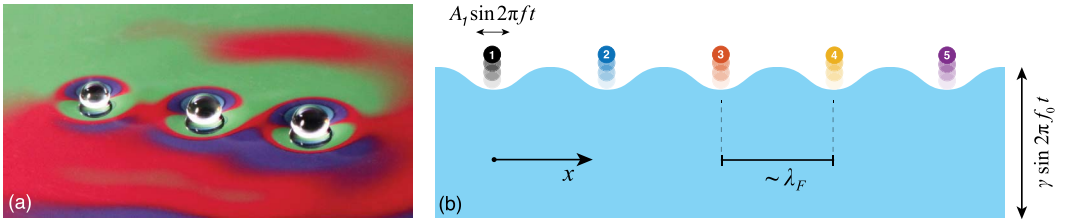

Figure 1. (a) A chain of three droplets bouncing on a vertically vibrating fluid bath. Photo credit: Daniel M. Harris. (b) Schematic of a periodically-forced chain of five droplets, as considered in Section 4. The first drop is forced sinusoidally in the horizontal direction with amplitude A_1 and frequency f, and the bath is vibrated vertically with peak acceleration γ and frequency f_0. The Faraday wavelength is denoted λ_F. Drops 1, 2, 3, 4 and 5 are indicated in black, blue, red, yellow, and purple, respectively, a color scheme that is repeated throughout the manuscript.

$\boldsymbol{F} = -(k_0 + k_1 \sin\omega t)\boldsymbol{x}$ could be probed. Periodic forcing of such droplets was also achieved by oscillating a magnet nearby (Supplementary Figure 3 in [8]).

The paper is organized as follows. In Section 2 we describe our theoretical model for the horizontal dynamics of droplets bouncing in resonance with the waves they generate. In Section 3 we investigate the structure and stability of free droplet chains. In Section 4 we present the results of a theoretical and numerical investigation of periodically-driven droplet chains. Future directions are discussed in Section 5.

2. The stroboscopic model

Consider a chain of N droplets with positions $x_i(t)$ constrained to move along a single line (Figure 1(b)). The droplets have mass m and radius R, and bounce in-phase on the surface of a bath of the same fluid in the presence of a gravitational acceleration g. The bath is subjected to a vertical acceleration $\gamma\sin(2\pi f_0 t)$, and has surface tension σ, density ρ, kinematic viscosity ν, and depth H. Provided $\gamma < \gamma_F$, with γ_F being the Faraday instability threshold [48], the surface of the bath would remain flat if not for the presence of the drops. We assume the droplets to be in a so-called $(2,1)$ bouncing mode, where the (i,j) notation indicates that the drop's vertical motion has period equal to i driving periods, and within this period the drop contacts the bath j times [49]. The drops' bouncing period $T_F = 2/f_0$ is thus equal to the bath's least stable Faraday mode [50–52], whose wavelength $\lambda_F = 2\pi/k_F$ may be approximated by the water-wave dispersion relation $(\pi f_0)^2 = (gk_F + \sigma k_F^3/\rho)\tanh(k_F H)$ for this system [53].

Following the theoretical developments of Moláček and Bush [53], we assume that the drops move in response to two forces: a wave force $-mgh'(x_i,t)$ proportional to the local slope of the wave field $h(x,t)$, and a drag $-D\dot{x}_i$ induced during impact and flight. Averaging the horizontal forces over the bouncing period yields an integro-differential trajectory equation for the droplets' horizontal positions [54]:

$$m\ddot{x}_i + D\dot{x}_i = -mgh'(x_i,t), \quad h(x,t) = \frac{A}{T_F}\sum_{j=1}^{N}\int_{-\infty}^{t} \mathrm{J}_0[k_F(x - x_j(s))]\mathrm{e}^{-(t-s)/T_M}\,\mathrm{d}s. \tag{1}$$

The drops are assumed to generate monochromatic standing waves with spatial profile $\mathrm{J}_0(k_F x)$ and decay time T_M, where J_0 is a Bessel function of the first kind. We assume the wave field to be linear, so that $h(x,t)$ may be expressed as the sum of waves generated prior to time t. The wave field in (1) is obtained by approximating the resulting discrete sum as an integral, an

approximation that is valid provided the timescale of horizontal motion is much greater than the bouncing period, $\lambda_F/|\dot{x}_p| \gg T_F$, as is the case in the experiments. The trajectory equation (1) is referred to as the *stroboscopic model*, as we have effectively eliminated consideration of the drops' vertical motion by averaging over the vertical dynamics, and model the drops as continuous moving sources of standing waves.

The drag coefficient D, memory time T_M and wave amplitude A are given by the formulas [27, 53]

$$D = Cmg\sqrt{\frac{\rho R}{\sigma}} + 6\pi\mu_a R\left(1 + \frac{\rho_a g R}{12\mu_a f}\right), \quad T_M = \frac{T_d}{1-\gamma/\gamma_F}$$

and

$$A = \frac{\sqrt{8\pi\nu_e T_F}}{3}\frac{(k_F R)^3}{3k_F^2\sigma/(\rho g)+1}\sin\Phi. \tag{2}$$

Here, C is a dimensionless drag constant, ρ_a and μ_a are the density and dynamic viscosity of air, respectively, T_d is the viscous decay time of the surface waves in the absence of forcing, ν_e is the bath's effective kinematic viscosity [53, 55] and $\sin\Phi$ is the sine of the droplet's impact phase. The first term in the formula for D results from the drag induced on the drop during its impact, the second from its free flight. Note that the memory time T_M increases as $\gamma \to \gamma_F$ from below, a regime in which the standing waves are more persistent. The terms "memory" and bath forcing acceleration are thus used interchangeably in what follows.

For the sake of simplicity, we neglect the effect of spatial damping, the exponential decay of surface waves in the far field that has been characterized experimentally [27, 56] and theoretically [57–59]. We also neglect the dependence of the impact phase $\sin\Phi$ on both the forcing acceleration γ and the instantaneous wave height, effects that have been quantified in recent experiments [60]. Impact phase variations have been shown to influence the stability of the orbital [61] and promenade [62] modes executed by pairs of walking droplets, and of free rings of bouncers [40]. We here restrict our attention to a relatively narrow range of forcing accelerations γ, for which we expect the constant-phase stroboscopic model (1) to capture the qualitative behavior of bouncing droplet chains.

We proceed by non-dimensionalizing the trajectory equation using the Faraday wavelength and memory time, and so let $x \to k_F x$ and $t \to t/T_M$ in (1). The dimensionless trajectory equation is thus

$$\kappa\ddot{x}_i + \dot{x}_i = \beta\sum_{j=1}^{N}\int_{-\infty}^{t} \mathrm{J}_1(x_i(t)-x_j(s))\mathrm{e}^{-(t-s)}\,\mathrm{d}s, \quad i = 1,\dots,N, \tag{3}$$

where $\kappa = m/DT_M$ is the dimensionless mass and $\beta = mgAk_F^2T_M^2/DT_F$ the dimensionless wave force coefficient. For this study, we adopt fluid parameters comparable to those used in typical experiments [4, 7, 38, 40, 53]. Specifically, we assume that the fluid bath of depth $H = 4$ mm consists of silicone oil with viscosity $\nu = 20$ cSt driven at $f_0 = 80$ Hz, with associated Faraday wavelength $\lambda_F = 4.75$ mm and viscous decay time $T_d = 0.018$ s. We also assume the droplets to have radius $R = 0.4$ mm and mass $m = 0.25$ mg, for which the time-averaged drag is $D = 2.0$ mg/s and wave amplitude $A = 3.5$ μm through (2). We adopt the value $\sin\Phi = 0.2$, which is roughly consistent with experimental measurements of the impact phase [60] and also provides adequate agreement between the predicted and observed speeds of walking droplets [53, 54]. For these parameter values, we obtain the formulas $\kappa \approx 7(1-\gamma/\gamma_F)$ and $\beta \approx 0.1/(1-\gamma/\gamma_F)^2$.

The present study is concerned with chains of bouncers, so we restrict our attention to the parameter regime $0.65 < \gamma/\gamma_F < 0.78$. According to the regime diagrams presented by Moláček and Bush [53] and Wind-Willassen *et al.* [63], the lower bound corresponds to the onset of the $(2,1)$ bouncing mode for drops with vibration number $2\pi f_0/\sqrt{\sigma/\rho R^3} \approx 0.86$. The upper

bound corresponds to the walking threshold $\beta = 2$ for a single drop [54], specifically, the critical vibrational acceleration above which the bouncing state destabilizes into a steadily translating walking state.

3. Free droplet chains

We proceed by investigating the structure and stability of free chains of bouncing droplets. The general framework is presented in Section 3.1, and the special case of a chain of $N = 5$ droplets is considered in Section 3.2.

3.1. *Stability of a chain of bouncers*

We first consider an equilibrium state of bouncers located at the fixed positions $x_i(t) = \chi_i$, where $\chi_i < \chi_j$ for $i < j$. Substituting this into (3), we find that the positions χ_i satisfy the system of equations $\sum_{j=1}^{N} \mathrm{J}_1(\chi_i - \chi_j) = 0$ for $i = 1, \ldots, N$. These conditions imply that the horizontal component of the wave force on each drop vanishes. Defining the inter-drop distances $d_i = \chi_{i+1} - \chi_i$ for $i = 1, \ldots, N-1$, we obtain an equivalent system of equations

$$-\sum_{j=1}^{i-1} \mathrm{J}_1\left(\sum_{k=j}^{i-1} d_k\right) + \sum_{j=i}^{N-1} \mathrm{J}_1\left(\sum_{k=i}^{j} d_k\right) = 0, \quad i = 1, \ldots, N-1. \tag{4}$$

These equations may be summed to obtain the corresponding equation for $i = N$.

We now assess the stability of this equilibrium bouncing state. To that end, we linearize the governing equations by substituting $x_i(t) = \chi_i + \epsilon \tilde{x}_i(t)$ into (3) and retaining terms at leading order in ϵ. Dropping the tildes in what follows, we obtain the linear system

$$\kappa \ddot{x}_i + \dot{x}_i = \beta \sum_{j=1}^{N} \mathrm{J}_1'(\chi_i - \chi_j) \int_{-\infty}^{t} (x_i(t) - x_j(s)) \mathrm{e}^{-(t-s)} \, \mathrm{d}s. \tag{5}$$

This may be recast as a system of ordinary differential equations by introducing the variables $X_i(t) = \int_{-\infty}^{t} x_i(s) \mathrm{e}^{-(t-s)} \, \mathrm{d}s$:

$$\kappa \ddot{x}_i + \dot{x}_i = \beta \sum_{j=1}^{N} \mathrm{J}_1'(\chi_i - \chi_j)(x_i - X_j), \quad \dot{X}_i = -X_i + x_i. \tag{6}$$

We may write (6) as a system of first-order ordinary differential equations, $\dot{\boldsymbol{z}} = Q\boldsymbol{z}$, where $\boldsymbol{z} = (x_1, \ldots, x_N, X_1, \ldots, X_N, \dot{x}_1, \ldots, \dot{x}_N)$. The matrix Q has the block form

$$Q = \begin{pmatrix} Z & Z & I \\ I & -I & Z \\ \frac{\beta}{\kappa} S & -\frac{\beta}{\kappa} P & -\frac{1}{\kappa} I, \end{pmatrix}, \quad \text{where } P_{ij} = \mathrm{J}_1'(\chi_i - \chi_j), \quad S_{ij} = \delta_{ij} \sum_{k=1}^{N} \mathrm{J}_1'(\chi_i - \chi_k), \tag{7}$$

Z is the $N \times N$ zero-matrix, I the $N \times N$ identity matrix and δ_{ij} the Kronecker delta. The stability of the bouncing state defined by (4) is determined by the eigenvalue s^* of Q with the largest real part. Specifically, the state is stable if $\mathrm{Re}(s^*) < 0$, and unstable otherwise. Note that one eigenvalue of Q is identically zero and is thus neglected from consideration; indeed, the corresponding eigenvector $(\mathbf{1}, \mathbf{1}, \mathbf{0})$ reflects the translation invariance of the trajectory equation (3), $\mathbf{1}$ and $\mathbf{0}$ being vectors in $\mathbb{R}^N$ of ones and zeros, respectively.

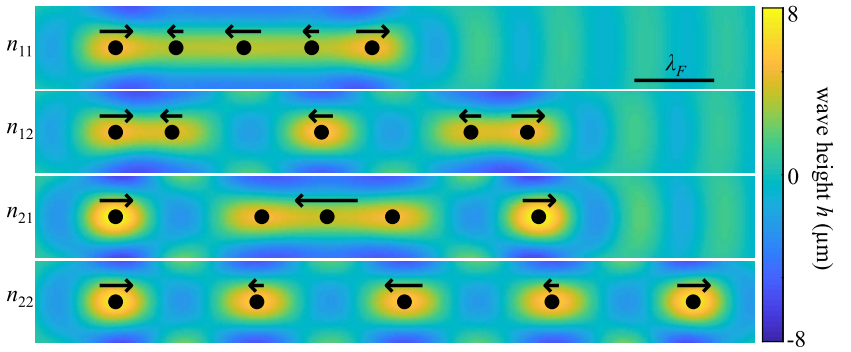

Figure 2. Schematic of the four symmetric bouncing states n_{11}, n_{12}, n_{21} and n_{22} described in Section 3.2. The colormap indicates the corresponding wave field $h(\boldsymbol{x}) = (AT_M/T_F)\sum_{i=1}^{N} \mathrm{J}_0(k_F|\boldsymbol{x} - (\chi_i, 0)|)$ at the onset of the chain's oscillatory instability. Black dots indicate the drop positions χ_i, as determined by solving (8). The eigenvector $\boldsymbol{z}^*$ corresponding to the unstable mode is depicted by the arrows; the size of the arrow indicates the magnitude of each component of $\boldsymbol{z}^*$, and the direction the approximate phase. The components of $\boldsymbol{z}^*$ for drops 2 and 4 in the n_{21}-state are small and thus not depicted. The scale bar shows the Faraday wavelength λ_F.

3.2. *Symmetric five-droplet chain*

We now consider the stability of *symmetric* chains of $N = 5$ bouncers, which satisfy the conditions $d_1 = d_4$ and $d_2 = d_3$. Such a configuration is particularly convenient for analysis, since equation (4) reduces to a system of two equations in the unknowns d_1 and d_2:

$$\begin{aligned} F_1(d_1, d_2) &\equiv \mathrm{J}_1(d_1) + \mathrm{J}_1(d_1 + d_2) + \mathrm{J}_1(d_1 + 2d_2) + \mathrm{J}_1(2d_1 + 2d_2) = 0, \\ F_2(d_1, d_2) &\equiv -\mathrm{J}_1(d_1) + \mathrm{J}_1(d_2) + \mathrm{J}_1(2d_2) + \mathrm{J}_1(d_1 + 2d_2) = 0. \end{aligned} \tag{8}$$

This system can readily be solved numerically, as its solutions correspond to the intersections of the zero-level curves of F_1 and F_2 (Supplementary Figure 1). These bouncing states are color-coded according to their stability at the lowest value of the forcing acceleration considered, $\gamma/\gamma_F = 0.66$, as is deduced by computing the eigenvalues of the matrix Q in (7), with blue (red) denoting stable (unstable) solutions. The stable equilibria may be labeled as n_{ij}, where the indices i and j denote increasing values of the inter-drop distances d_1 and d_2, respectively.

For the remainder of the paper, we will restrict our attention to the four bouncing states n_{11}, n_{12}, n_{21} and n_{22}, as depicted in Figure 2. The results of the linear stability analysis of these bouncing states are presented in Supplementary Figure 2. The real part of the least stable eigenvalue s^* increases with the forcing acceleration γ, and the imaginary part is nonzero, indicating that each of these states goes unstable to an oscillatory instability as γ is increased progressively. The instability threshold is the lowest for the state n_{11}; this result may be understood on the basis of the fact that the oscillation amplitude of the wave kernel $\mathrm{J}_0(k_F x)$ decreases with x, indicating that the force between droplets generally weakens as the distance between them increases.

The eigenvector $\boldsymbol{z}^*$ corresponding to the unstable mode at the onset of instability ($\mathrm{Re}(s^*) = 0$) is depicted by the arrows in Figure 2. We note that each of the bouncing states exhibits a qualitatively similar unstable mode, with the drops in the interior oscillating roughly out-of-phase with respect to the ones at the edges. The second and fourth drops exhibit weaker oscillations than the others, and remain roughly stationary for the n_{21}-bouncing state. With the exception of the n_{12}-state, the drop in the middle exhibits the strongest oscillations, with

oscillation amplitudes nearly twice that of the drops on the edges for the n_{21}-state. This result is qualitatively consistent with the observation of Eddi *et al.* [32], who conducted experiments on quasi-1D aggregates of bouncers consisting of more than ten drops along one direction and three drops in the transverse direction. They observed that the aggregates effectively "melt" from the center as the bath's vibrational acceleration is increased progressively, in contrast to classical melting processes that occur along the edges of a material.

The oscillation frequency of the droplet chain (Supplementary Figure 2(c)) is obtained by numerically computing the eigenvalues of the matrix Q in (7). An estimate for these frequencies may be obtained by considering the simplified case of two drops interacting in the low-memory regime, for which we may approximate $X_i \approx x_i$ in (6). The linearized equation (6) then assumes the form of a spring-mass system with dimensionless mass κ and spring constant $-\beta \mathrm{J}_1'(d)$, d being the equilibrium distance between the drops that satisfies $\mathrm{J}_1(d) = 0$. The effective frequency of oscillation is thus $f = \sqrt{\beta|\mathrm{J}_1'(d)|/\kappa}/(2\pi)$, which has the dimensional form

$$f = \frac{1}{2\pi}\sqrt{\frac{Ak_F^2|\mathrm{J}_1'(k_F d)|gT_M}{T_F}}. \tag{9}$$

Using the value of T_M for $\gamma/\gamma_F = 0.74$, which corresponds to the onset of instability for the n_{11}-state (Supplementary Figure 2(a)), and the separation distance $d/\lambda_F = 0.61$, which corresponds to the first nonzero solution of $\mathrm{J}_1(k_F d) = 0$, we obtain the frequency $f = 1.3$ Hz from (9). This result agrees well with the experimental results of Eddi *et al.* [32], who measured oscillation frequencies of $f = 1$ Hz for quasi-1D and 2D hexagonal lattices, and $f = 1.3$ Hz for 2D square lattices.

4. Forced droplet chains

We now investigate the response of a droplet chain to a time-periodic forcing applied to the drop at one end, as depicted in Figure 1(b). Specifically, we assume that the horizontal motion of the first drop is prescribed, $x_1(t) = A_1 \sin(2\pi f t)$, where the oscillation amplitude A_1 and frequency f are given. As in Section 3.2, we restrict our attention to the four equilibrium states n_{11}, n_{12}, n_{21} and n_{22} depicted in Figure 2, and pay particular attention to the state n_{11} for which the drops are closest to each other, $d_1 \approx d_2 \approx 0.8\lambda_F$. We consider the parameter regime $0.66 \le \gamma/\gamma_F \le 0.74$, the lower bound corresponding to the onset of the $(2,1)$ resonant bouncing mode (see Section 2), and the upper bound being just above the onset of the oscillatory instability for the n_{11}-bouncing state (Supplementary Figure 2(a)). We also assume the forcing frequency to be much less than the bouncing frequency $f_0/2 = 40$ Hz, $f \ll f_0/2$, a regime in which we expect the bouncing dynamics to remain periodic and thus the stroboscopic model (3) to remain valid. Specifically, we restrict our attention to the regime $fT_M \le 0.3$, which corresponds to forcing frequencies less than 6 Hz for $\gamma/\gamma_F \ge 0.66$.

4.1. *Linear theory of forced droplet chains*

We begin by assessing the linear response of a droplet chain to a small periodic forcing, $A_1 \ll \lambda_F$. To that end, we define $\omega = 2\pi f$ and substitute $x_i(t) = A_i e^{i\omega t}$ and $X_i(t) = A_i e^{i\omega t}/(1+i\omega)$ into the linear equation (6), which describes the small-amplitude oscillations of a chain of bouncers around their equilibrium positions. We thus obtain a linear system of equations for the complex amplitudes A_i, which may be written in the matrix form $M\boldsymbol{a} = \boldsymbol{v}$, where $\boldsymbol{a} = (A_2, \ldots, A_N)/A_1$.

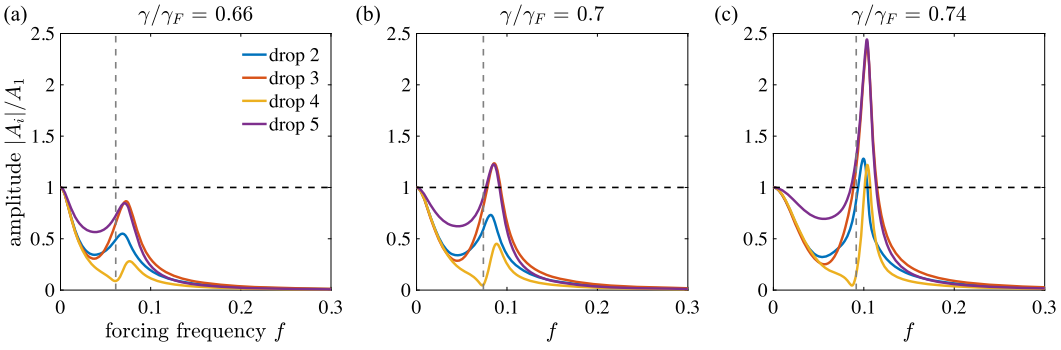

Figure 3. Dependence of the oscillation amplitude $|A_i|$ on the dimensionless forcing frequency f for a chain of five drops initialized in the n_{11}-bouncing state, as predicted by the linear theory described in Section 4.1 (10). The amplitudes are normalized by the forcing amplitude A_1 applied to the first drop. The colors correspond to the different drops in the chain, as indicated by the legend in panel (a). Three values of the bath's forcing acceleration are shown: (a) $\gamma/\gamma_F = 0.66$, (b) $\gamma/\gamma_F = 0.7$ and (c) $\gamma/\gamma_F = 0.74$. The dashed gray lines denote the resonant frequency of an unforced droplet chain, as approximated by (9).

Here, M is a $(N-1)\times(N-1)$ matrix and $\boldsymbol{v}$ a vector in $\mathbb{C}^{N-1}$ with entries

$$M_{ij} = \begin{cases} -\kappa\omega^2 + \mathrm{i}\omega - \beta\left(\sum_{k\neq i}^{N-1} \mathrm{J}_1'(\chi_{i+1}-\chi_{k+1}) + \mathrm{J}_1'(\chi_{i+1}) + \dfrac{\mathrm{i}\omega}{1+\mathrm{i}\omega}\mathrm{J}_1'(0)\right) & \text{if } i = j \\ \dfrac{\beta}{1+\mathrm{i}\omega}\mathrm{J}_1'(\chi_{i+1}-\chi_{j+1}) & \text{if } i \neq j, \end{cases} \tag{10}$$

$$v_i = -\frac{\beta}{1+\mathrm{i}\omega}\mathrm{J}_1'(\chi_{i+1}).$$

Figure 3 shows the dependence of the amplitudes $|A_i|/A_1$ on the forcing frequency f for a chain of five drops initialized in the n_{11}-bouncing state. The corresponding results for the other bouncing states n_{12}, n_{21} and n_{22} are shown in Supplementary Figure 3. The qualitative features of the curves in Figure 3 and Supplementary Figure 3 may be interpreted on the basis of the oscillatory modes depicted in Figure 2. Specifically, for the n_{11} and n_{22} states, drops 3 and 5 exhibit substantially larger oscillation amplitudes than drops 2 and 4. This is not so for the other bouncing states; specifically, all of the drops exhibit comparable oscillation amplitudes for the n_{12}-state, and drops 2 and 4 have rather low amplitudes for the n_{21}-state (Supplementary Figure 3).

Note that $|A_i|/A_1 \to 1$ in the limit $f \to 0$, which is evident from inspection of (10). Moreover, $|A_i|/A_1 \to 0$ in the high-frequency limit $f \to \infty$, a regime that will be treated in Section 4.3. For intermediate values of the forcing frequency, the oscillation amplitudes are maximized for a critical value of the forcing frequency. This resonant frequency is approximated well by the characteristic frequency of a droplet pair in the low-memory limit, as given by (9) and depicted by the dashed lines in Figure 3. Moreover, the maximum amplitude increases with memory and may exceed the imposed amplitude A_1 (Figures 3(b) and 3(c)). This result suggests that relatively large-amplitude oscillations may be excited for forcing frequencies near the droplet chain's intrinsic resonant frequency, particularly as the waves become more persistent. While the theory presented in this section is strictly valid for small-amplitude oscillations, such resonant oscillations will be revisited using numerical simulations of droplet chains, the results of which are presented in the next section.

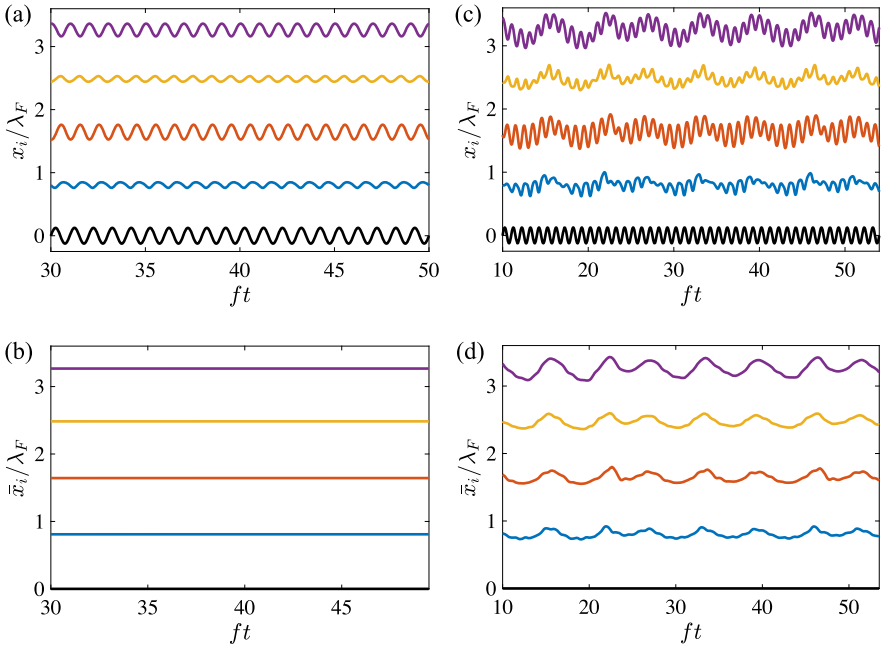

Figure 4. Numerical solutions of the trajectory equation (3) for a chain of $N = 5$ drops initialized in the n_{11}-bouncing state. The first drop (black curve) is subjected to a periodic forcing of amplitude $A_1 = \lambda_F/8$. Panels (a) and (c) show the drop trajectories $x_i(t)$, the time ft given in units of the forcing period $T = 1/f$. Panels (b) and (d) show the cycle-averaged drop position $\bar{x}_i(t)$, as defined in (11). Simple periodic oscillations are evident in panels (a) and (b), corresponding to $f = 0.08$ and bath vibrational acceleration $\gamma/\gamma_F = 0.7$. Aperiodic oscillations are shown in panels (c) and (d), corresponding to $f = 0.09$ and $\gamma/\gamma_F = 0.74$. The frequencies f correspond to those for which the third and fifth drops exhibit the largest oscillations, as shown in Figures 5(b) and 5(c).

4.2. *Nonlinear oscillations of forced droplet chains*

While the linear equation (10) is straightforward to solve, numerical simulations of the trajectory equation (3) are required to assess the nonlinear response of a droplet chain to finite-amplitude oscillations. To that end, we adapt the numerical method described by Oza *et al.* [64] to solve (3), which consists of using a fourth-order Adams–Bashforth method for time-stepping combined with Simpson's rule for the integrals. The histories of each drop must also be specified, which we take to correspond to an equilibrium bouncing state, specifically, $x_i(t) = \chi_i$ for $t < 0$, where the constants χ_i are determined by solving (8). The trajectories are evolved up to a final time $t_{\max} \geq \max(50T, 600)$, and the dimensionless time step is taken to be $\Delta t = \min(2^{-4}, T/40)$, where $T = 1/f$ is the forcing period.

Simulated trajectories for a droplet chain initialized in the n_{11}-bouncing state are shown in Figure 4. At relatively low memory, the drops exhibit simple oscillations (Figure 4(a)). Note that the drop at the end of the chain (purple) oscillates roughly in-phase with the forced drop (black), and roughly out-of-phase with respect to the drops in the interior, which is consistent with the predictions of the linear stability analysis of unforced chains presented in Figure 2. At higher memory, the drops often exhibit complex aperiodic oscillations, as shown in Figure 4(c). To

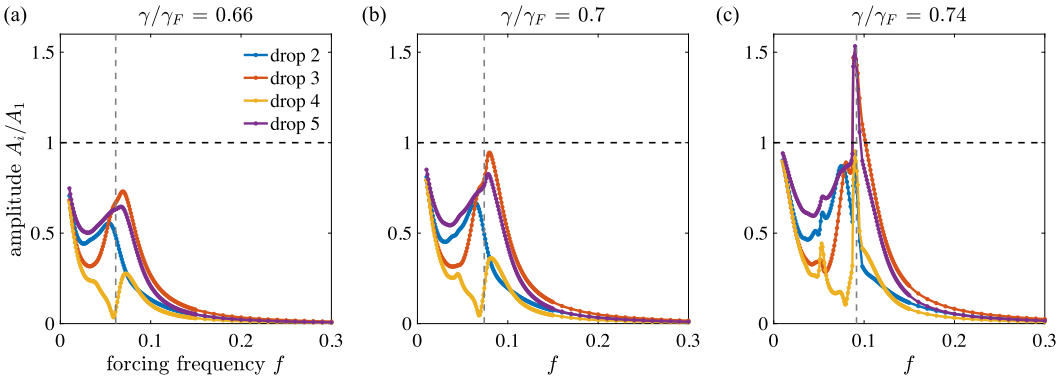

Figure 5. Dependence of the oscillation amplitude A_i on the dimensionless forcing frequency f for a chain of five drops initialized in the n_{11}-bouncing state, as obtained from numerical simulations of the trajectory equation (3). The amplitudes are normalized by the forcing amplitude $A_1 = \lambda_F/8$ applied to the first drop. The colors correspond to the different drops in the chain, as indicated by the legend in panel (a). Three values of the bath's forcing acceleration are shown: (a) $\gamma/\gamma_F = 0.66$, (b) $\gamma/\gamma_F = 0.7$ and (c) $\gamma/\gamma_F = 0.74$. The dashed gray lines denote the resonant frequency of an unforced droplet chain, as approximated by (9).

characterize the envelope of the oscillations, we define the cycle-averaged drop position

$$\bar{x}_i(t) = \frac{1}{T}\int_{t-T/2}^{t+T/2} x_i(s)\,\mathrm{d}s. \tag{11}$$

This quantity is constant for the simple oscillatory motion occurring at low memory (Figure 4(b)), but exhibits oscillations on a timescale long relative to the forcing period T for the complex motion arising at higher memory (Figure 4(d)).

To quantify the dependence of the oscillation amplitude A_i of each drop on the forcing frequency f, we define

$$A_i = \left[\frac{2}{t_0}\int_{t_{\max}-t_0}^{t_{\max}} (x_i(t) - \langle x_i\rangle)^2\,\mathrm{d}t\right]^{1/2}, \quad \text{where } \langle x_i\rangle = \frac{1}{t_0}\int_{t_{\max}-t_0}^{t_{\max}} x_i(t)\,\mathrm{d}t \tag{12}$$

and $t_0 \leq 5T$. Figure 5 shows the oscillation amplitudes A_i/A_1 of a droplet chain in the n_{11}-bouncing state, with the first drop subjected to a forcing amplitude $A_1 = \lambda_F/8$. We note that the predictions of the linear theory (Figure 3) are qualitatively consistent with the simulations; specifically, the oscillation amplitude of each drop is maximized for a critical value of the forcing frequency f, which is approximated well by (9) (gray dashed line). Moreover, the maximum oscillation amplitude increases with memory. At the highest memory considered, $\gamma/\gamma_F = 0.74$, the amplitudes of drops 3 and 5 exceed that of the first drop. This indicates that a vibrating chain of droplets can effectively draw energy from the surface waves and thus execute oscillations whose amplitude exceeds that which is imposed. We note that the maximum amplitudes in simulations (Figure 5) are smaller than those predicted by the linear theory (Figure 3), indicating that nonlinear effects serve to effectively damp the forced oscillations. Similar conclusions may be drawn for droplet chains forced in the n_{12}, n_{21} and n_{22}-bouncing states, the results for which are shown in Supplementary Figures 4(a)–(c), 4(d)–(f) and 4(g)–(i), respectively.

Figure 6 shows the results for a droplet chain initialized in the n_{11}-bouncing state and forced with a larger amplitude, $A_1 = \lambda_F/4$. The behavior is qualitatively different from that predicted by the linear theory (Figure 3); specifically, the second drop (blue) rather than the third (red) exhibits

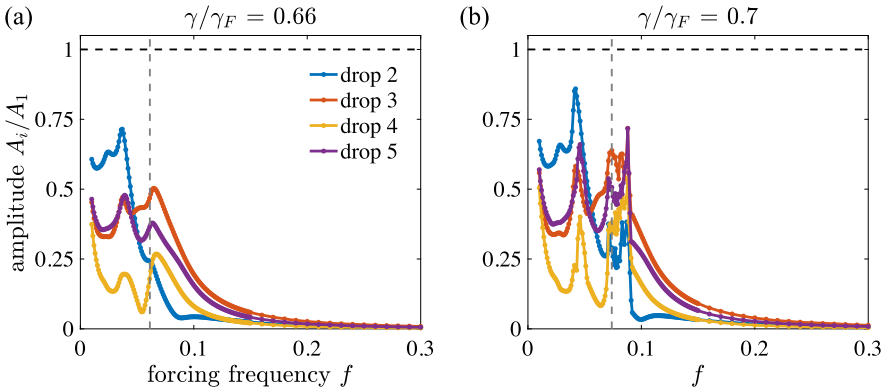

Figure 6. The procedure described in the caption of Figure 5 is repeated for a larger value of the forcing amplitude, $A_1 = \lambda_F/4$.

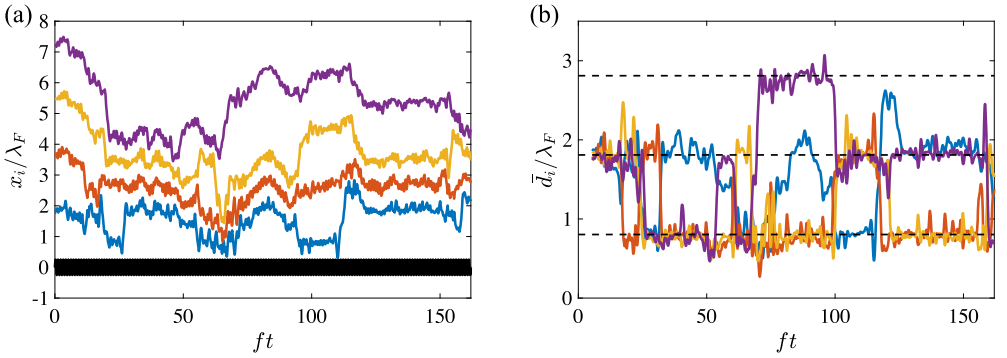

Figure 7. Complex aperiodic oscillations observed in a chain of $N = 5$ drops initialized in the n_{22}-bouncing state on a bath with vibrational forcing acceleration $\gamma/\gamma_F = 0.74$. The first drop (black) is subjected to a periodic forcing of amplitude $A_1 = \lambda_F/4$ and dimensionless frequency $f = 0.09$. (a) Trajectories $x_i(t)$ of each drop, plotted as a function of the dimensionless time ft. (b) Cycle-averaged inter-drop distances $\bar{d}_i(t) = \bar{x}_{i+1}(t) - \bar{x}_i(t)$ for $i = 1$ (blue), 2 (red), 3 (yellow) and 4 (purple). The dashed lines indicate the mean inter-drop distances $(d_1 + d_2)/2$ of the symmetric unforced bouncing states n_{11}, n_{22} and n_{33}, as given by (8).

the largest oscillations for a critical forcing frequency f, which in turn is overestimated by the approximate formula (9) (gray dashed line). Moreover, the oscillation amplitudes may exhibit maxima at multiple values of the forcing frequency f even at low memory (Figure 6(a)), an effect absent at the lower forcing amplitude (Figure 5(a)). The results for higher memory are not shown because the simulated trajectories exhibit intersections in this parameter regime for certain values of the forcing frequency f. These unphysical solutions are an artifact of the stroboscopic model's poor characterization of the waves in the near field. Indeed, the model (1) was derived under the assumption that the drops are point sources of waves [53], an approximation that is known to be inadequate when the distance between the drops is comparable to their diameter [61].

For relatively large memory and forcing amplitude A_1, the droplets execute aperiodic and presumably chaotic trajectories, as shown in Figure 7(a). To understand the qualitative features of this complex dynamics, we plot in Figure 7(b) the cycle-averaged distances between neighboring

drops, $\bar{d}_i(t) = \bar{x}_{i+1}(t) - \bar{x}_i(t)$, where $\bar{x}_i(t)$ is defined in (11). The dashed lines indicate the mean inter-drop distances $(d_1 + d_2)/2$ of the symmetric unforced bouncing states n_{11}, n_{22} and n_{33}, as predicted by (8). We observe that $\bar{d}_i(t)$ exhibits oscillations around the dashed lines, punctuated by intermittent transitions between them. Unlike the solutions observed for lower forcing amplitude A_1 (Figure 4), the droplet chain chaotically jumps between different equilibrium solutions without settling near any of them.

4.3. *High-frequency limit $f \to \infty$*

As shown in Figures 3, 5 and 6, the drops' oscillation amplitudes go to zero in the limit of large forcing frequency, $A_i \to 0$ as $f \to \infty$. In this limit, we find that the chain effectively settles into a new bouncing state that is dynamically stabilized by the periodic forcing applied to the first drop. To rationalize this observation, we substitute into (3) the expressions $x_1(t) = A_1 \sin\omega t$ and $x_i(t) = \chi_i$ for $i = 2, \dots, N$, where $\omega = 2\pi f$, and obtain

$$\frac{1}{\omega}\int_0^\infty \mathrm{J}_1(\chi_i - A_1\sin(\tau-\sigma))\mathrm{e}^{-\sigma/\omega}\,\mathrm{d}\sigma + \sum_{j=2}^{N}\mathrm{J}_1(\chi_i-\chi_j) = 0, \tag{13}$$

where $\tau = \omega t$. Note that the integral in (13) is a 2π–periodic function of τ, and can be simplified in the limit $\omega \to \infty$:

$$\begin{aligned}\frac{1}{\omega}\int_0^\infty \mathrm{J}_1(\chi_i - A_1\sin(\tau-\sigma))\mathrm{e}^{-\sigma/\omega}\,\mathrm{d}\sigma &= \frac{1}{\omega}\sum_{n=0}^{\infty}\mathrm{e}^{-2\pi n/\omega}\int_0^{2\pi}\mathrm{J}_1(\chi_i - A_1\sin(\tau-\sigma))\mathrm{e}^{-\sigma/\omega}\,\mathrm{d}\sigma \\ &= \frac{1}{\omega(1-\mathrm{e}^{-2\pi/\omega})}\int_0^{2\pi}\mathrm{J}_1(\chi_i - A_1\sin(\tau-\sigma))\mathrm{e}^{-\sigma/\omega}\,\mathrm{d}\sigma = \frac{1}{2\pi}\int_0^{2\pi}\mathrm{J}_1(\chi_i - A_1\sin\sigma)\,\mathrm{d}\sigma + O(\omega^{-1}),\end{aligned} \tag{14}$$

where the geometric series formula is used in the second line. The drop positions χ_i thus satisfy the following algebraic equation in the limit $\omega \to \infty$:

$$\frac{1}{2\pi}\int_0^{2\pi}\mathrm{J}_1(\chi_i - A_1\sin\sigma)\,\mathrm{d}\sigma + \sum_{j=2}^{N}\mathrm{J}_1(\chi_i-\chi_j) = 0, \quad i = 2,\dots,N. \tag{15}$$

We solve (15) using numerical continuation in the parameter A_1 starting from $A_1 = 0$, the corresponding solution being the n_{11}-bouncing state as defined by (8). Figure 8(a) shows the dependence of the inter-drop distances $d_i = \chi_{i+1} - \chi_i$ on the forcing amplitude A_1. While the distances d_2 (red), d_3 (orange) and d_4 (purple) remain roughly constant over the range of forcing amplitudes considered, the distance d_1 (blue) between drops 1 and 2 increases dramatically near $A_1/\lambda_F \approx 0.4$ and $A_1/\lambda_F \approx 0.8$, with plateaus in between. The plateaus are approximated well by the dashed lines in Figure 8(a), which denote the values of d_1 for unforced droplet chains, as predicted by (4). Specifically, the dashed line with the lowest value of $d_1 \approx 0.8\lambda_F$ corresponds to the n_{11} symmetric bouncing state, whereas the other lines with $d_1 \approx 1.3\lambda_F$ and $d_1 \approx 1.8\lambda_F$ correspond to asymmetric bouncing states, for which $d_1 \neq d_4$ and $d_2 \neq d_3$.

We proceed by assessing the stability of the unforced bouncing states (dashed lines in Figure 8(a)) for the lowest memory considered, $\gamma/\gamma_F = 0.66$, using the procedure described in Section 3.1. Specifically, we find the eigenvalues of the matrix Q in (7), and find that states with $d_1 \approx 0.8\lambda_F$ and $d_1 \approx 1.8\lambda_F$ (black dashed lines) are stable, whereas the one with $d_1 \approx 1.3\lambda_F$ (gray dashed line) is unstable. Note that the wave field associated with the unstable bouncing state has a relatively large amplitude at the positions of the first and second drop (Figure 8(c)), as compared to the stable n_{11}-state (Figure 8(b)) and the dynamically stabilized state (Figure 8(d)), where the wave field of a droplet chain forced in the limit of high frequency $f \to \infty$ is given by

$$h(x) = \frac{AT_M}{T_F}\left[\frac{1}{2\pi}\int_0^{2\pi}\mathrm{J}_0(k_F(x - A_1\sin\sigma))\,\mathrm{d}\sigma + \sum_{j=2}^{N}\mathrm{J}_0(k_F(x-\chi_j))\right]. \tag{16}$$

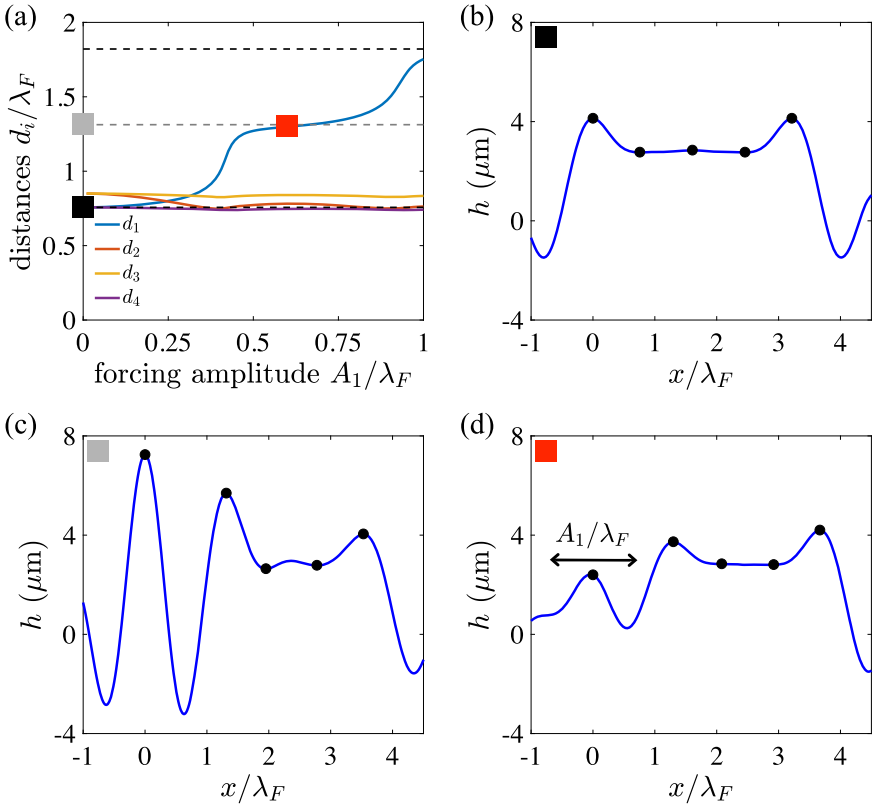

Figure 8. Bouncing states of a chain of five drops forced in the limit of high frequency, $f \to \infty$. (a) The dependence of the inter-drop distances $d_i = x_{i+1} - x_i$ on the forcing amplitude A_1, as obtained by solving (15). The dashed lines denote the values of d_1 for an unforced droplet chain, black (gray) lines corresponding to stable (unstable) solutions for $\gamma/\gamma_F = 0.66$. Panels (b)–(d) show the wave profiles $h(x)$ in microns, as given by (16) (blue curves), and drop positions (black dots), corresponding to three configurations: (b) an unforced stable chain in the n_{11}-bouncing state (black square), (c) an unforced unstable chain (gray square), and (d) a chain forced with amplitude $A_1/\lambda_F = 0.6$ (red square).

The physical picture is that high-frequency forcing applied to the first drop may be used to drive transitions between bouncing states, wherein the distance d_1 between the first two drops increases in increments of size roughly $\lambda_F/2$ as the forcing amplitude A_1 is increased progressively, and the distances between the other drops remain roughly constant. Moreover, an unstable bouncing state may be effectively stabilized by a high-frequency periodic forcing of sufficiently large amplitude A_1, which leads to a wave field of diminished amplitude at the position of the second drop. We note that dynamical stabilization of bouncing states through a qualitatively similar mechanism is observed for droplet chains initialized in the n_{12}, n_{21} and n_{22}-states, as shown in Supplementary Figure 5.

5. Discussion

We have presented the results of a theoretical and numerical investigation into chains of bouncing droplets. We have characterized the equilibrium configurations of chains of five droplets, and

found that they go unstable to an oscillatory instability as the bath's forcing acceleration γ/γ_F is increased progressively. We have observed that, with the exception of the n_{12}-bouncing state, the drop in the middle of the chain exhibits the largest oscillations at the onset of the instability (Figure 2). These results are qualitatively consistent with the experiments of Eddi *et al.* [32], who found that quasi-1D aggregates of bouncers effectively melt from the interior at a critical value of the bath's forcing acceleration. We have also derived an approximation (9) for the oscillation frequency of a droplet chain at the onset of the instability, whose associated prediction $f \approx 1$ Hz agrees well with the observations of Eddi *et al.* [32].

We have found that droplet chains may exhibit a complex dynamics when the drop at one end is subjected to sinusoidal forcing in the horizontal direction. Specifically, simple oscillatory motion is observed at relatively low memory (Figures 4(a) and 4(b)), while complex aperiodic behavior is observed at higher memory (Figures 4(c) and 4(d)). As is evident by comparing Figures 3 and 5, the dependence of the drop oscillation amplitude A_i on the forcing frequency f is described well by the linear theory presented in Section 4.1, provided the forcing amplitude A_1 on the first drop is relatively small, $A_1 \ll \lambda_F$. The dependence of A_i on f is more complex for larger values of A_1 (Figure 6), a regime in which nonlinear effects are expected to play an important role. At relatively high memory, the drops may oscillate with an amplitude larger than that prescribed (Figure 5(c)), $A_i > A_1$, suggesting that the drops effectively extract energy from the collective wave field and convert it to kinetic energy.

At the largest forcing amplitude A_1 and memory considered, periodic forcing may be used as a mechanism to generate chaotic dynamics (Figure 7(a)). In this regime, the droplet chain exhibits intermittent oscillations between the different bouncing states without settling near any of them (Figure 7(b)). This physical picture of a walker jumping chaotically between states has been reported in a number of settings, for example, in a rotating frame [7, 64], harmonic potential [8–10, 65], and circular [12, 13] and elliptical corrals [14]. While a walker's dynamics under periodic forcing has received less attention, Perrard [47] subjected a walker to a periodically oscillating central force, $\boldsymbol{F} = -(k_0 + k_1 \sin\omega t)\boldsymbol{x}$, and observed transitions between circular orbits and lemniscates for suitable values of k_1 and ω.

In the limit in which the applied oscillation frequency of the first drop is large, $f \to \infty$, new bouncing states may be dynamically stabilized provided the forcing amplitude A_1 is sufficiently large (Figure 8(a)). This phenomenon is similar to the so-called Kapitza pendulum, in which a fast oscillation of the pivot point stabilizes the upward vertical position of the pendulum and destabilizes the downward vertical position [41, 42, 66]. We note that dynamic stabilization of unstable quantum states has also been achieved experimentally, for example in potassium Rydberg atoms subjected to strong pulsed electric fields [67] and atomic Bose–Einstein condensates subjected to periodic microwave pulses [68].

Our results indicate that a droplet chain exhibiting relatively large-amplitude oscillations may be viewed as a damped oscillator forced near resonance. Equation (6), which describes the linear small-amplitude oscillations of a chain of bouncers around their equilibrium positions, may thus be compared with the equations of motion of spring-mass-damper chains, which comprise a series of masses connected by linear springs and subjected to friction forces [69]. This analogy was noted by Borghesi *et al.* [70] in their study of promenading pairs of walking droplets. However, three significant differences are evident: first, the damping term $\dot{x}_i$ in the droplet chain is due to a drag, and thus depends only on the velocity of each particle instead of the particles' relative velocities $\dot{x}_i - \dot{x}_j$. Second, the interactions are long-range, unlike the nearest-neighbor interactions of spring-mass-damper chains: each drop experiences a wave field that results from the sum of the waves generated by all other drops. Third, the drops are coupled by a fluid-mediated memory and thus temporally nonlocal forces, as the wave force on each droplet is due to the waves generated in each droplet's past. Mathematically, the forces are not proportional

to the difference $x_i - x_j$, as for linear springs, but rather to $x_i - X_j$, where X_j is an exponentially-weighted integral of the position of drop j. In the low-memory regime, the effective spring constant is proportional to the memory time T_M, as is evident from (9). The drop oscillation amplitude increases with T_M (Figures 5 and 6), a behavior consistent with the fact that the resonant oscillation amplitude in mass-spring systems increases with the spring constant [69]. We note that spring-mass lattices are the basic model for the description of phonons in crystalline solids [33], and that analogues of phonons have also been observed in a 1D microfluidic crystal, which consists of a chain of immiscible drops in a liquid-filled channel [71].

It is our hope that the theoretical predictions presented herein may be validated experimentally, a possible avenue being the protocol described by Perrard [47] for periodically forcing droplets using an oscillating magnetic field. Longer droplet chains ($N \gg 5$) may also be studied theoretically, although the model (1) would need to be modified to account for the exponential decay of the surface waves in the far field [40]. A worthwhile future direction would be to explore hydrodynamic analogues of Floquet engineering [45], wherein a time-dependent forcing is tuned in order to control a quantum system. While the present study was restricted to chains of bouncers forced sinusoidally at one end, different forms of periodic forcing could be used to control the structure and dynamics of more complex bouncing droplet lattices.

Acknowledgments

The second author is supported by the CNRS Momentum funding program. The last author is supported by the Simons Foundation (Collaboration Grant for Mathematicians, Award No. 587006).

Supplementary data

Supporting information for this article is available on the journal's website under https://doi.org/10.5802/crmeca.30 or from the author.

References

[1] J. Walker, "Drops of liquid can be made to float on the liquid. What enables them to do so?", *Sci. Am.* **238** (1978), 151.
[2] Y. Couder, E. Fort, C.-H. Gautier, A. Boudaoud, "From bouncing to floating: noncoalescence of drops on a fluid bath", *Phys. Rev. Lett.* **94** (2005), 177801.
[3] Y. Couder, S. Protière, E. Fort, A. Boudaoud, "Walking and orbiting droplets", *Nature* **437** (2005), 208.
[4] S. Protière, A. Boudaoud, Y. Couder, "Particle-wave association on a fluid interface", *J. Fluid Mech.* **554** (2006), p. 85-108.
[5] A. Eddi, E. Fort, F. Moisy, Y. Couder, "Unpredictable tunneling of a classical wave-particle association", *Phys. Rev. Lett.* **102** (2009), 240401.
[6] E. Fort, A. Eddi, J. Moukhtar, A. Boudaoud, Y. Couder, "Path-memory induced quantization of classical orbits", *Proc. Natl. Acad. Sci.* **107** (2010), no. 41, p. 17515-17520.
[7] D. M. Harris, J. W. M. Bush, "Drops walking in a rotating frame: From quantized orbits to multimodal statistics", *J. Fluid Mech.* **739** (2014), p. 444-464.
[8] S. Perrard, M. Labousse, M. Miskin, E. Fort, Y. Couder, "Self-organization into quantized eigenstates of a classical wave-driven particle", *Nat. Commun.* **5** (2014), 3219.
[9] S. Perrard, M. Labousse, E. Fort, Y. Couder, "Chaos driven by interfering memory", *Phys. Rev. Lett.* **113** (2014), 104101.
[10] S. Perrard, M. Labousse, "Transition to chaos in wave memory dynamics in a harmonic well: Deterministic and noise-driven behavior", *Chaos* **28** (2018), 096109.
[11] A. Eddi, J. Moukhtar, S. Perrard, E. Fort, Y. Couder, "Level splitting at a macroscopic scale", *Phys. Rev. Lett.* **108** (2012), 264503.
[12] D. M. Harris, J. Moukhtar, E. Fort, Y. Couder, J. W. M. Bush, "Wavelike statistics from pilot-wave dynamics in a circular corral", *Phys. Rev. E* **88** (2013), 011001.

[13] T. Cristea-Platon, P. J. Sáenz, J. W. M. Bush, "Walking droplets in a circular corral: Quantisation and chaos", *Chaos* **28** (2018), 096116.
[14] P. J. Sáenz, T. Cristea-Platon, J. W. M. Bush, "Statistical projection effects in a hydrodynamic pilot-wave system", *Nat. Phys.* **14** (2018), p. 315-319.
[15] P. J. Sáenz, T. Cristea-Platon, J. W. M. Bush, "A hydrodynamic analog of Friedel oscillations", *Sci. Adv.* **6** (2020), 20.
[16] R. Valani, A. C. Slim, T. Simula, "Hong-Ou-Mandel-like two-drop correlations", *Chaos* **28** (2018), 096104.
[17] Y. Couder, E. Fort, "Single particle diffraction and interference at a macroscopic scale", *Phys. Rev. Lett.* **97** (2006), 154101.
[18] A. Andersen, J. Madsen, C. Reichelt, S. R. Ahl, B. Lautrup, C. Ellegaard, M. T. Levinsen, T. Bohr, "Double-slit experiment with single wave-driven particles and its relation to quantum mechanics", *Phys. Rev. E* **92** (2015), 013006.
[19] T. Bohr, A. Andersen, B. Lautrup, "Bouncing droplets, pilot-waves, and quantum mechanics", in *Recent Advances in Fluid Dynamics with Environmental Applications* (J. Klapp, L. D. G. Sigalotti, A. Medina, A. López, G. Ruiz-Chavarría, eds.), Springer International Publishing, Switzerland, 2016, p. 335-349.
[20] R. Dubertrand, M. Hubert, P. Schlagheck, N. Vandewalle, T. Bastin, J. Martin, "Scattering theory of walking droplets in the presence of obstacles", *New J. Phys.* **18** (2016), 113037.
[21] G. Pucci, D. M. Harris, L. M. Faria, J. W. M. Bush, "Walking droplets interacting with single and double slits", *J. Fluid Mech.* **835** (2018), p. 1136-1156.
[22] M. Rode, J. Madsen, A. Andersen, "Wave fields in double-slit experiments with wave-driven droplets", *Phys. Rev. Fluids* **4** (2019), 104801.
[23] C. Ellegaard, M. T. Levinsen, "Interaction of wave-driven particles with slit structures", *preprint*, arXiv:2005.12335 (2020).
[24] Y. Couder, E. Fort, "Probabilities and trajectories in a classical wave-particle duality", *J. Phys.: Conf. Ser.* **361** (2012), 012001.
[25] J. W. M. Bush, "Pilot-wave hydrodynamics", *Ann. Rev. Fluid Mech.* **47** (2015), p. 269-292.
[26] J. W. M. Bush, "The new wave of pilot-wave theory", *Phys. Today* **68** (2015), no. 8, p. 47-53.
[27] A. Eddi, E. Sultan, J. Moukhtar, E. Fort, M. Rossi, Y. Couder, "Information stored in Faraday waves: the origin of a path memory", *J. Fluid Mech.* **674** (2011), p. 433-463.
[28] A. Eddi, A. Decelle, E. Fort, Y. Couder, "Archimedean lattices in the bound states of wave interacting particles", *Europhys. Lett.* **87** (2009), 56002.
[29] S. Protière, Y. Couder, E. Fort, A. Boudaoud, "The self-organization of capillary wave sources", *J. Phys.: Condens. Matter* **17** (2005), 3529.
[30] S. I. Lieber, M. C. Hendershott, A. Pattanaporkratana, J. E. Maclennan, "Self-organization of bouncing oil drops: two dimensional lattices and spinning clusters", *Phys. Rev. E* **75** (2007), 56308.
[31] A. Eddi, D. Terwagne, E. Fort, Y. Couder, "Wave propelled ratchets and drifting rafts", *Europhys. Lett.* **82** (2008), 44001.
[32] A. Eddi, A. Boudaoud, Y. Couder, "Oscillating instability in bouncing drop crystals", *Euro. Phys. Lett.* **94** (2011), 20004.
[33] C. Kittel, *Introduction to Solid State Physics, Vol. 8*, Wiley, New York, 1976.
[34] P. J. Sáenz, G. Pucci, A. Goujon, T. Cristea-Platon, J. Dunkel, J. W. M. Bush, "Spin lattices of walking droplets", *Phys. Rev. Fluids* **3** (2018), 100508.
[35] P. J. Sáenz, G. Pucci, S. E. Turton, A. Goujon, R. R. Rosales, J. Dunkel, J. W. M. Bush, "Emergent order in hydrodynamic spin lattices", (2020) (submitted).
[36] B. Filoux, M. Hubert, N. Vandewalle, "Strings of droplets propelled by coherent waves", *Phys. Rev. E* **92** (2015), 041004(R).
[37] A. Rahman, "Standard map-like models for single and multiple walkers in an annular cavity", *Chaos* **28** (2018), 096102.
[38] S. J. Thomson, M. M. P. Couchman, J. W. M. Bush, "Collective vibrations of confined levitating droplets", *Phys. Rev. Fluids* **5** (2020), 083601.
[39] S. J. Thomson, M. Durey, R. R. Rosales, "Collective vibrations of a hydrodynamic active lattice", *Proc. R. Soc. A* **476** (2020), no. 2239.
[40] M. M. P. Couchman, J. W. M. Bush, "Free rings of bouncing droplets: stability and dynamics", *J. Fluid Mech.* (2020) https://doi.org/10.1017/jfm.2020.648 (in press).
[41] P. L. Kapitza, "Dynamical stability of a pendulum when its point of suspension vibrates", in *Collected Papers of P. L. Kapitza, Vol. 2* (D. Ter Haar, ed.), Pergamon, Oxford, UK, 1965, p. 714-725.
[42] P. L. Kapitza, "Pendulum with a vibrating suspension", in *Collected Papers of P. L. Kapitza, Vol. 2* (D. Ter Haar, ed.), Pergamon, Oxford, UK, 1965, p. 726-737.
[43] L. Gammaitoni, P. Hänggi, P. Jung, F. Marchesoni, "Stochastic resonance", *Rev. Mod. Phys.* **70** (1998), no. 1, p. 223-287.
[44] P. Hänggi, "Driven quantum systems", in *Quantum Transport and Dissipation* (T. Dittrich, P. Hänggi, G.-L. Ingold, G. Schön, W. Zwerger, eds.), Wiley-VCH, New York, 1998, p. 249-286.
[45] M. Bukov, L. D'Aless, A. Polkovnikov, "Universal high-frequency behavior of periodically driven systems: from dynamical stabilization to Floquet engineering", *Adv. Phys.* **64** (2015), no. 2, p. 139-226.

[46] F. L. Traversa, M. Di Ventra, F. Bonani, "Generalized Floquet theory: Application to dynamical systems with memory and Bloch's theorem for nonlocal potentials", *Phys. Rev. Lett.* **110** (2013), 170602.
[47] S. Perrard, Une mémoire ondulatoire: Etats propres, Chaos et Probabilités. PhD thesis, Université Paris Diderot, 2014, p. 182-183.
[48] M. Faraday, "On the forms and states of fluids on vibrating elastic surfaces", *Phil. Trans. R. Soc. Lond.* **121** (1831), p. 319-340.
[49] T. Gilet, J. W. M. Bush, "The fluid trampoline: droplets bouncing on a soap film", *J. Fluid Mech.* **625** (2009), p. 167-203.
[50] T. B. Benjamin, F. Ursell, "The stability of the plane free surface of a liquid in vertical periodic motion", *Proc. R. Soc. Lond. A* **225** (1954), p. 505-515.
[51] K. Kumar, L. S. Tuckerman, "Parametric instability of the interface between two fluids", *J. Fluid Mech.* **279** (1994), p. 49-68.
[52] K. Kumar, "Linear theory of Faraday instability in viscous liquids", *Proc. R. Soc. A* **452** (1996), p. 1113-1126.
[53] J. Moláček, J. W. M. Bush, "Drops walking on a vibrating bath: towards a hydrodynamic pilot-wave theory", *J. Fluid Mech.* **727** (2013), p. 612-647.
[54] A. U. Oza, R. R. Rosales, J. W. M. Bush, "A trajectory equation for walking droplets: hydrodynamic pilot-wave theory", *J. Fluid Mech.* **737** (2013), p. 552-570.
[55] A. Prosperetti, "Viscous effects on small-amplitude surface waves", *Phys. Fluids* **19** (1976), no. 2, p. 195-203.
[56] A. P. Damiano, P.-T. Brun, D. M. Harris, C. A. Galeano-Rios, J. W. M. Bush, "Surface topography measurements of the bouncing droplet experiment", *Exp. Fluids* **57** (2016), 163.
[57] P. A. Milewski, C. Galeano-Rios, A. Nachbin, J. W. M. Bush, "Faraday pilot-wave dynamics: modelling and computation", *J. Fluid Mech.* **778** (2015), p. 361-388.
[58] S. E. Turton, M. M. P. Couchman, J. W. M. Bush, "A review of the theoretical modeling of walking droplets: towards a generalized pilot-wave framework", *Chaos* **28** (2018), 096111.
[59] L. Tadrist, J.-B. Shim, T. Gilet, P. Schlagheck, "Faraday instability and subthreshold Faraday waves: surface waves emitted by walkers", *J. Fluid Mech.* **848** (2018), p. 906-945.
[60] M. M. P. Couchman, S. E. Turton, J. W. M. Bush, "Bouncing phase variations in pilot-wave hydrodynamics and the stability of droplet pairs", *J. Fluid Mech.* **871** (2019), p. 212-243.
[61] A. U. Oza, E. Siéfert, D. M. Harris, J. Moláček, J. W. M. Bush, "Orbiting pairs of walking droplets: Dynamics and stability", *Phys. Rev. Fluids* **2** (2017), 053601.
[62] J. Arbelaiz, A. U. Oza, J. W. M. Bush, "Promenading pairs of walking droplets: Dynamics and stability", *Phys. Rev. Fluids* **3** (2018), 013604.
[63] Ø. Wind-Willassen, J. Moláček, D. M. Harris, J. W. M. Bush, "Exotic states of bouncing and walking droplets", *Phys. Fluids* **25** (2013), 082002.
[64] A. U. Oza, Ø. Wind-Willassen, D. M. Harris, R. R. Rosales, J. W. M. Bush, "Pilot-wave hydrodynamics in a rotating frame: Exotic orbits", *Phys. Fluids* **26** (2014), 082101.
[65] N. B. Budanur, M. Fleury, "State space geometry of the chaotic pilot-wave hydrodynamics", *Chaos* **29** (2019), 013122.
[66] L. D. Landau, E. M. Lifshitz, *Course of Theoretical Physics. Vol. 1: Mechanics*, Butterworth-Heinemann, Oxford, UK, 1976.
[67] C. O. Reinhold, J. Burgdörfer, M. T. Frey, F. B. Dunning, "Dynamic stabilization of the periodically kicked Rydberg atom", *Phys. Rev. Lett.* **79** (1997), 26.
[68] T. M. Hoang, C. S. Gerving, B. J. Land, M. Anquez, C. D. Hamley, M. S. Chapman, "Dynamic stabilization of a quantum many-body spin system", *Phys. Rev. Lett.* **111** (2013), 090403.
[69] S. S. Rao, *Mechanical Vibrations*, Addison Wesley, Harlow, Essex, UK, 1995.
[70] C. Borghesi, J. Moukhtar, M. Labousse, A. Eddi, E. Fort, Y. Couder, "Interaction of two walkers: Wave-mediated energy and force", *Phys. Rev. E* **90** (2014), 063017.
[71] T. Beatus, T. Tlusty, B.-Z. Roy, "Phonons in a one-dimensional microfluidic crystal", *Nat. Phys.* **2** (2006), no. 11, p. 743-748.